Online Supplementary Material

Tables S1–S5

Figures S1–S14

Table S1. Series detrending and chronology development. Characteristics of 32 ensemble runs performed with the ARSTAN software (Cook et al. 2005) and applied to the full and pruned MXD datasets (Table S2), resulting in a total of 64 slightly different MXD chronologies (considering the standard output option STD).

Ensemble Run	Detrending	Power Transform	RC Detrending	Index Calculation	Chronology Mean	Variance Correction
1	RCS	no	2/3 sl spline	ratios	mean	no
2	RCS	no	2/3 sl spline	ratios	bi-weight	no
3	RCS	no	2/3 sl spline	ratios	mean	rbar-weight
4	RCS	no	2/3 sl spline	ratios	bi-weight	rbar-weight
5	RCS	no	100yr spline	ratios	mean	no
6	RCS	no	100yr spline	ratios	bi-weight	no
7	RCS	no	100yr spline	ratios	mean	rbar-weight
8	RCS	no	100yr spline	ratios	bi-weight	rbar-weight
9	RCS	yes	2/3 sl spline	residuals	mean	no
10	RCS	yes	2/3 sl spline	residuals	bi-weight	no
11	RCS	yes	2/3 sl spline	residuals	mean	rbar-weight
12	RCS	yes	2/3 sl spline	residuals	bi-weight	rbar-weight
13	RCS	yes	100yr spline	residuals	mean	no
14	RCS	yes	100yr spline	residuals	bi-weight	no
15	RCS	yes	100yr spline	residuals	mean	rbar-weight
16	RCS	yes	100yr spline	residuals	bi-weight	rbar-weight
17	200yr spline	no	no	ratios	mean	no
18	200yr spline	no	no	ratios	bi-weight	no
19	200yr spline	no	no	ratios	mean	rbar-weight
20	200yr spline	no	no	ratios	bi-weight	rbar-weight

21	200yr spline	yes	no	residuals	mean	no
22	200yr spline	yes	no	residuals	bi-weight	no
23	200yr spline	yes	no	residuals	mean	rbar-weight
24	200yr spline	yes	no	residuals	bi-weight	rbar-weight
25	2/3 sl spline	no	no	ratios	mean	no
26	2/3 sl spline	no	no	ratios	bi-weight	no
27	2/3 sl spline	no	no	ratios	mean	rbar-weight
28	2/3 sl spline	no	no	ratios	bi-weight	rbar-weight
29	2/3 sl spline	PWT	no	residuals	mean	no
30	2/3 sl spline	PWT	no	residuals	bi-weight	no
31	2/3 sl spline	PWT	no	residuals	mean	rbar-weight
32	2/3 sl spline	PWT	no	residuals	bi-weight	rbar-weight

Table S2. Dataset characteristics. Comparison of the original and trimmed maximum latewood density (MXD in g/cm^3) datasets used for chronology development.

	Number of Series	**Start Year (CE)**	**End Year (CE)**	**Mean Series Length**	**Min Series Length**	**Max Series Length**	**Mean Series MXD**	**Min Series MXD**	**Max Series MXD**	**Mean Series AC1**	**Min Series AC1**	**Max Series AC1**
Original Dataset	534	924	2020	204	4	732	0.64	0.44	0.84	0.47	-0.61	0.88
Trimmed Dataset	494	924	2020	218	39	732	0.64	0.5	0.77	0.49	0.03	0.87

Table S3. Volcanic forcing. A total of 20 volcanic eruptions used for SEA. Estimated Northern Hemisphere (NH) volcanic forcing after Sigl et al. (2015) is expressed as watts per meter squared (W/m^2). Question marks in parentheses indicate uncertainty of the information given in the table.

Source Volcano	**Eruption Date**	**Evidence**	**VEI**	**NH Forcing**	**SEA Year 0**
Katla, Iceland (?)	1209 (?)	Tephra		1210 (-4.17)	1210

Unknown	1232 (?)	Ice Core		1230 (-11.28)	1232
Rinjani, Indonesia	1257 (?)	Ice Core	7	1258 (-18.09)	1258
Unknown	1287 (?)	Ice Core		1286 (-5.53)	1288
Unknown	1344 (?)	Ice Core		1345 (-5.58)	1345
Unknown	1452 (?)	Ice Core	6*	1453 (-4.96)	1453
Unknown	1458 (?)	Ice Core		1458 (-7.81)	1459
Unknown	1512 (?)	Ice Core		1512 (-3.33)	1513
Kelut, Indonesia (?)	1586	Documented	5*	1585 (-3.9)	1587
Huaynaputina, Peru	1600 (19 Feb)	Documented	6	1601 (-7.85)	1601
Parker, Philippines (?)	1641 (Jan)	Documented	5*	1641 (-8.85)	1643
Unknown	1698 (?)	Dendro		1695 (-5.73)	1698
Laki, Iceland	1783-4	Documented	6	1783 (-15.49)	1783
Unknown	1809	Ice Core	6	1809 (-6.93)	1809
Tambora, Indonesia	1815 (10 Apr)	Documented	7	1815 (-7.98)	1816
Babuyan Claro, Philippines (?)	1832	Ice Core		1832 (-5.61)	1833
Cosigüina, Nicaragua	1835 (20 Jan)	Documented	5	1836 (-4.65)	1835
Krakatau, Indonesia	1883 (26 Aug)	Documented	6	1884 (-3.39)	1884
Novarupta, Alaska	1912 (06 Jun)	Documented	6	1912 (-3.26)	1913
Pinatubo, Philippines	1991 (15 Jun)	Documented	6	1992 (-4.27)	1991

Table S4. Calibration-verification trials. Pearson (P Corr), Robust (R Corr) and Spearman S Corr) correlation coefficients, as well as the Coefficient of Efficiency (CoEf) and Reduction of Error (ReEr) statistics calculated for the full and two earl/late split calibration-(extra)verification periods of our new summer temperature reconstruction. Durban-Watson (DW) statistics were further calculated for the three calibration periods.

	P Corr	R Corr	S Corr	ReEr	CoEf	DW
Full Calibration (1920-2020)	0.71	0.69	0.66	0.49	0.49	1.81
Extra Verification (1870-1920)	0.66	0.65	0.62	0.43	0.43	--

Early Calibration (1920-1970)	0.67	0.67	0.68	0.45	0.45	1.86
Late Verification (1970-2020)	0.76	0.73	0.69	0.44	0.42	--
Late Calibration (1970-2020)	0.76	0.73	0.69	0.57	0.57	1.91
Early Verification (1920-1970)	0.67	0.67	0.68	0.34	0.31	--

Table S5. Military conflicts on the Iberian Peninsula that took place between Christians and Muslims and amongst Christians. The comprehensive inventory spans the period 1119–2020 CE and is provided as a separate excel file (uploaded).

--- uploaded separately ---

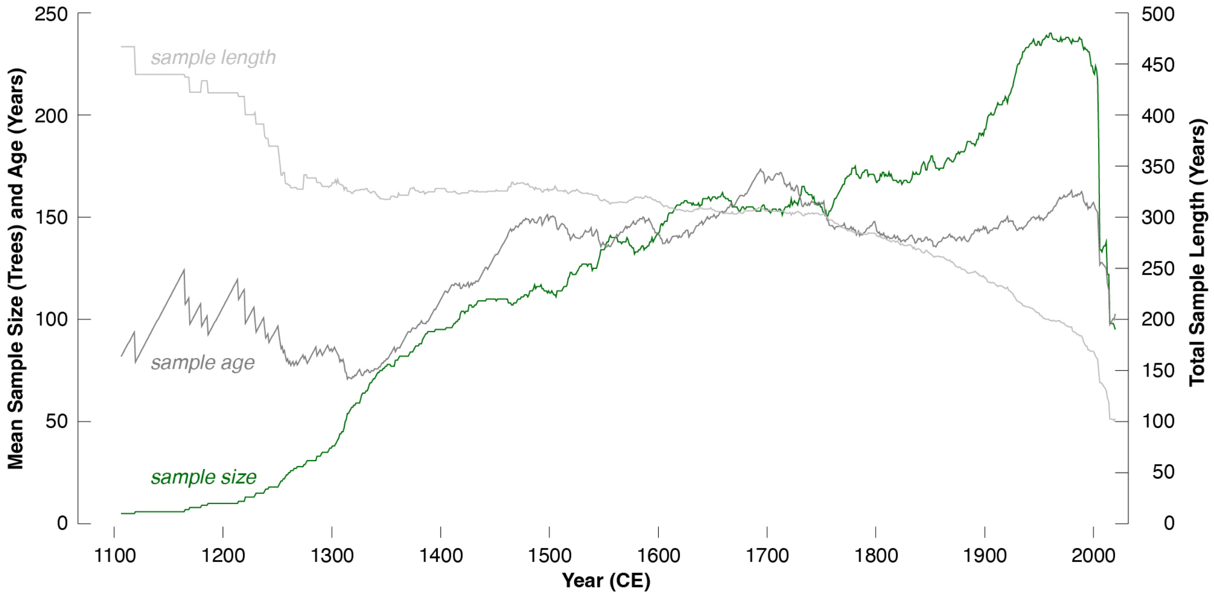

Figure S1. Sample characteristics. Average sample length, sample age and sample size between 1119 and 2020 CE.

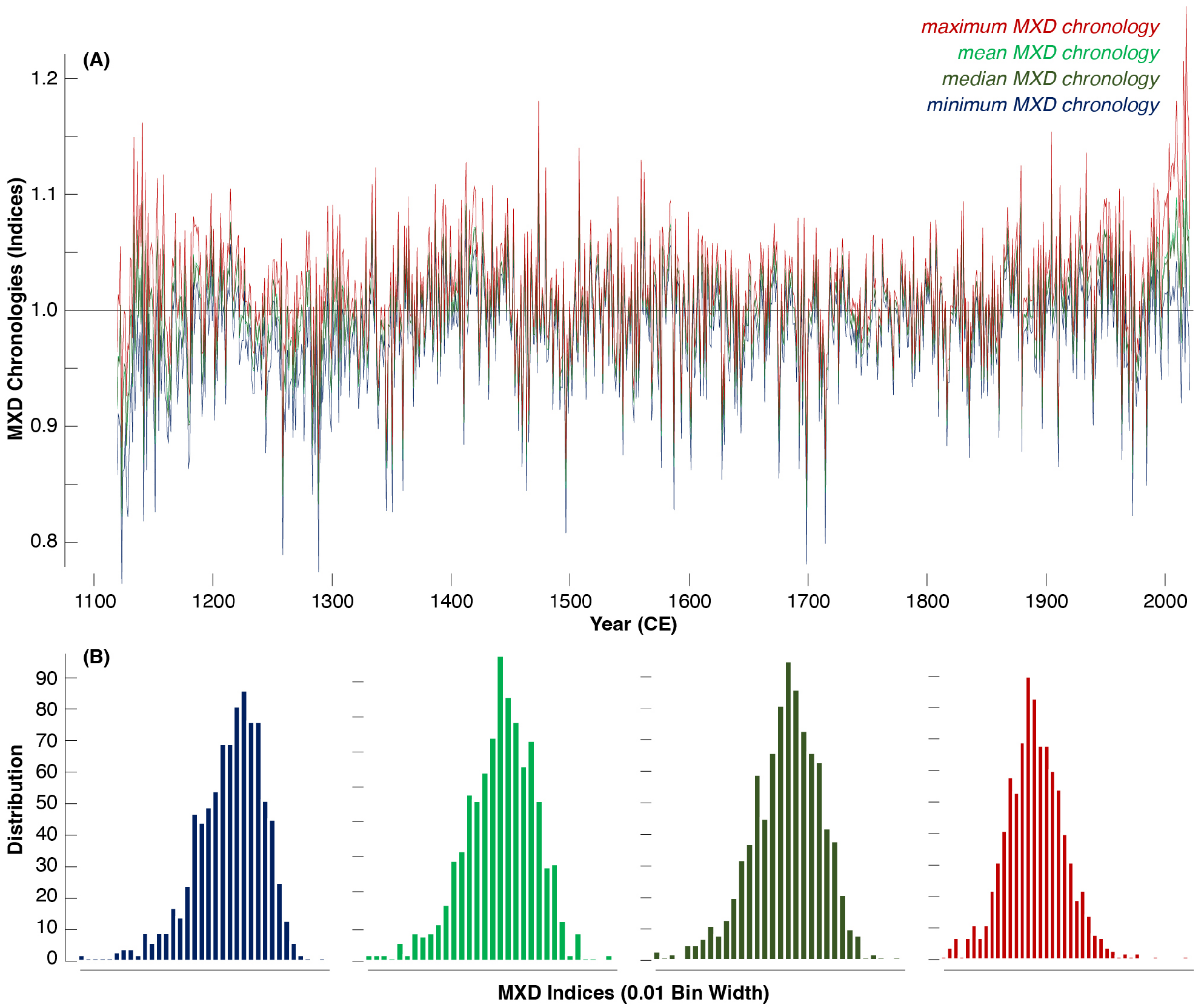

Figure S2. Chronology behaviour. (**A**) Comparison of the minimum, mean, median and maximum MXD chronologies between 1119 and 2020 CE. Mean values of the four chronologies are slightly different (0.98, 1.00, 1.00 and 1.01), whereas their standard deviation is similar (0.05). (**B**) Distribution plots of the 902 annual MXD indices of the four different chronologies indicating some bias towards lower values in all beside the maximum timeseries.

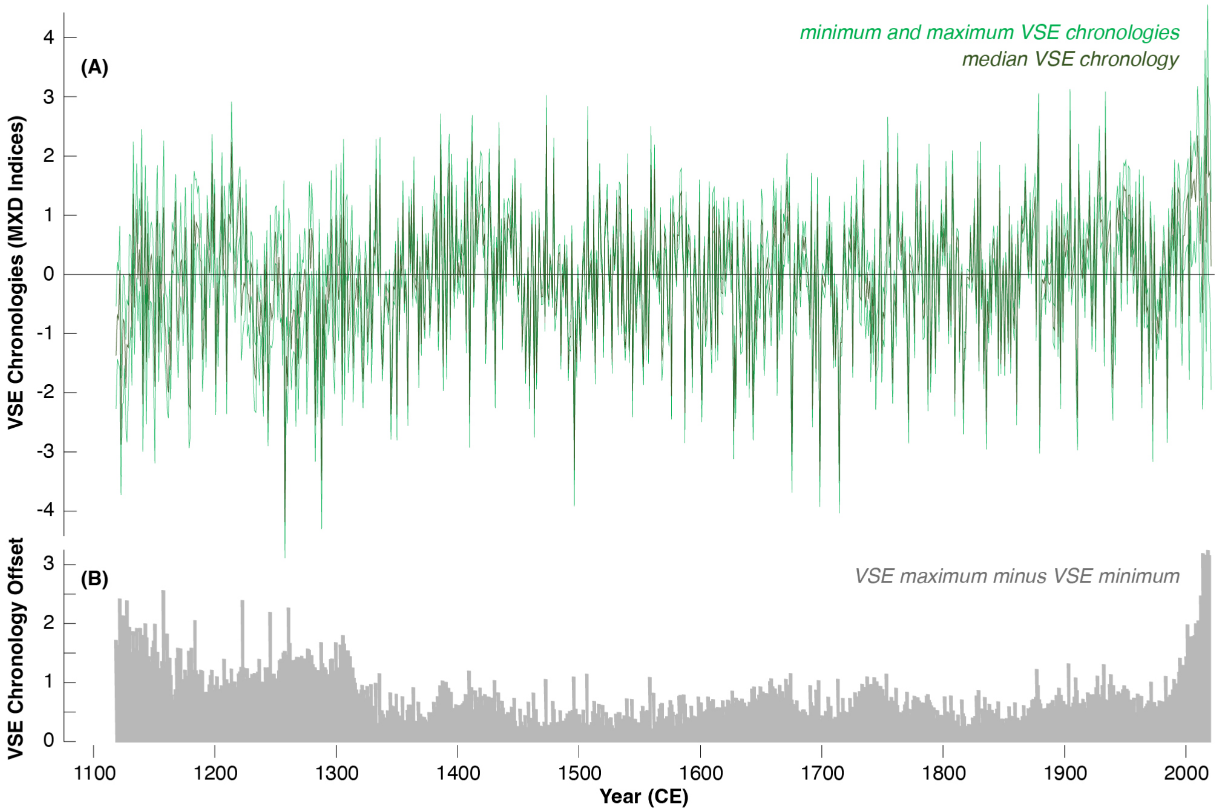

Figure S3. Chronology comparison. (**A**) The three final, minimum, median and maximum ensemble chronologies after variance stabilisation (VSE), spanning the period 1119–2020 CE and exhibiting the lowest and highest MXD estimates in 1258 and 2017 CE, respectively. (**B**) Annual differences between the minimum and maximum VSE MXD chronologies, which are included in the final error estimation.

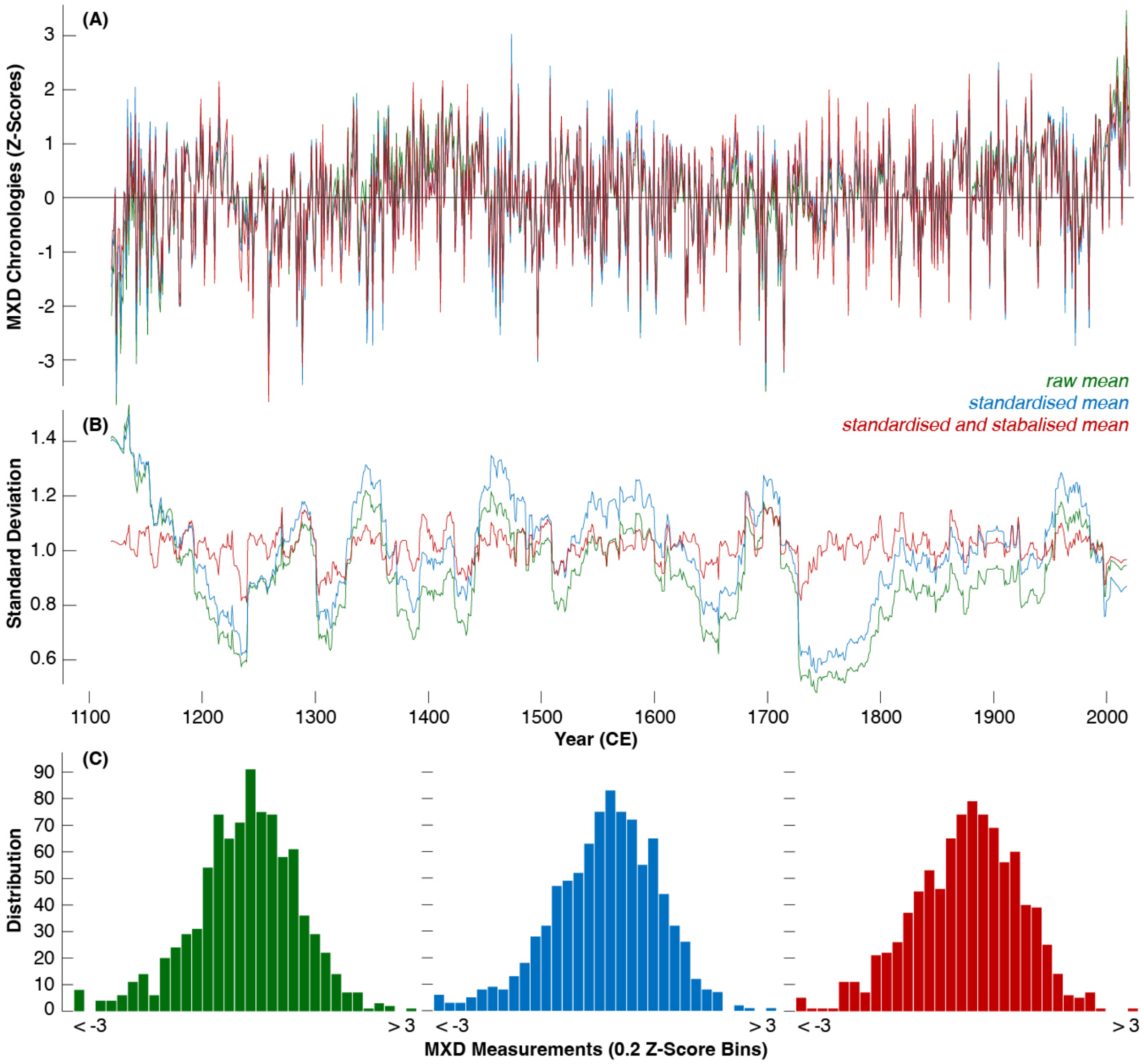

Figure S4. Variance changes. (**A**) Comparison of the mean of all raw maximum latewood density (MXD) measurements without any detrending (green), the mean of all 64 MXD chronology members of the ensemble approach (blue), and the variance stabilised ensemble mean (red). (**B**) Moving 31-year standard deviations of the three timeseries shown above, and (**C**) their corresponding density distributions. All timeseries were normalised to have a mean of 0 and a standard deviation of 1 over 1119–2020 CE.

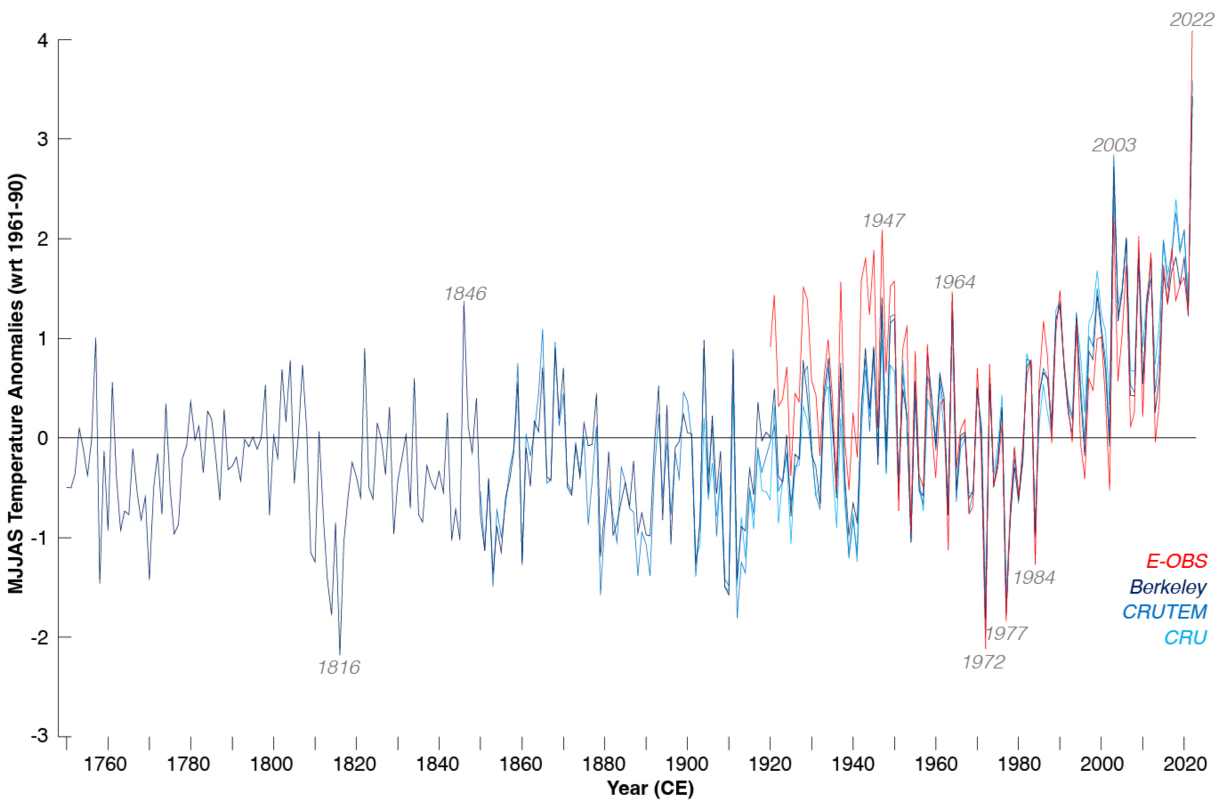

Figure S5. Gridded temperature changes. Comparison of four different gridded land surface May–September (MJJAS) temperature means for 42–43° North and 0–2° East (Fig. 1). All timeseries are expressed as anomalies with respect to 1961–1990 CE. The highest spatial resolution of 0.25° is achieved by E-OBS (v25.0e), which covers 1920–2022 (Cornes et al. 2018). Spatial resolution of 0.5° and 5.0° is provided by CRU (TS4.06) and CRUTEM (5.0), with their timeseries spanning 1901–2021 and 1850–2022 (Harris et al. 2020), respectively. The longest temperature data available at 1.0° spatial resolution from Berkeley extend back to 1750 CE (Rohde and Hausfather 2020).

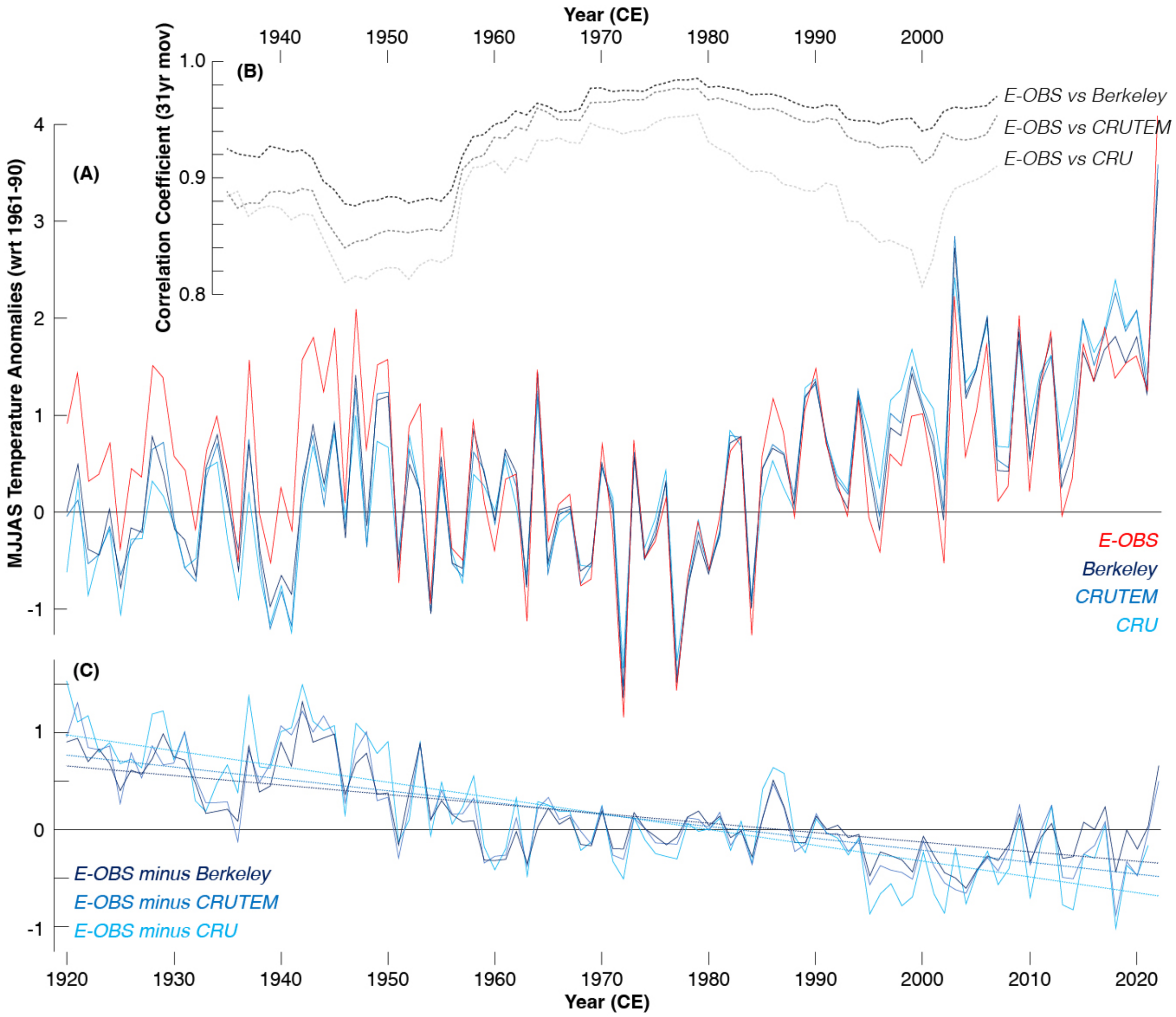

Figure S6. Gridded temperature offset. (**A**) Comparison of four different gridded land surface May–September (MJJAS) temperature means over their common 1920–2022 CE period. Measurements of the latest the E-OBS (v25.0e) product are generally warmer than all other data before circa 1950 CE, and slightly cooler since around the mid-1990. (**B**) Moving 31-year correlation coefficients and (**C**) linear trends of the residuals between the E-OBS measurements and the three other products by CRU (TS4.06), CRUTEM (5.0), and Berkeley (v23).

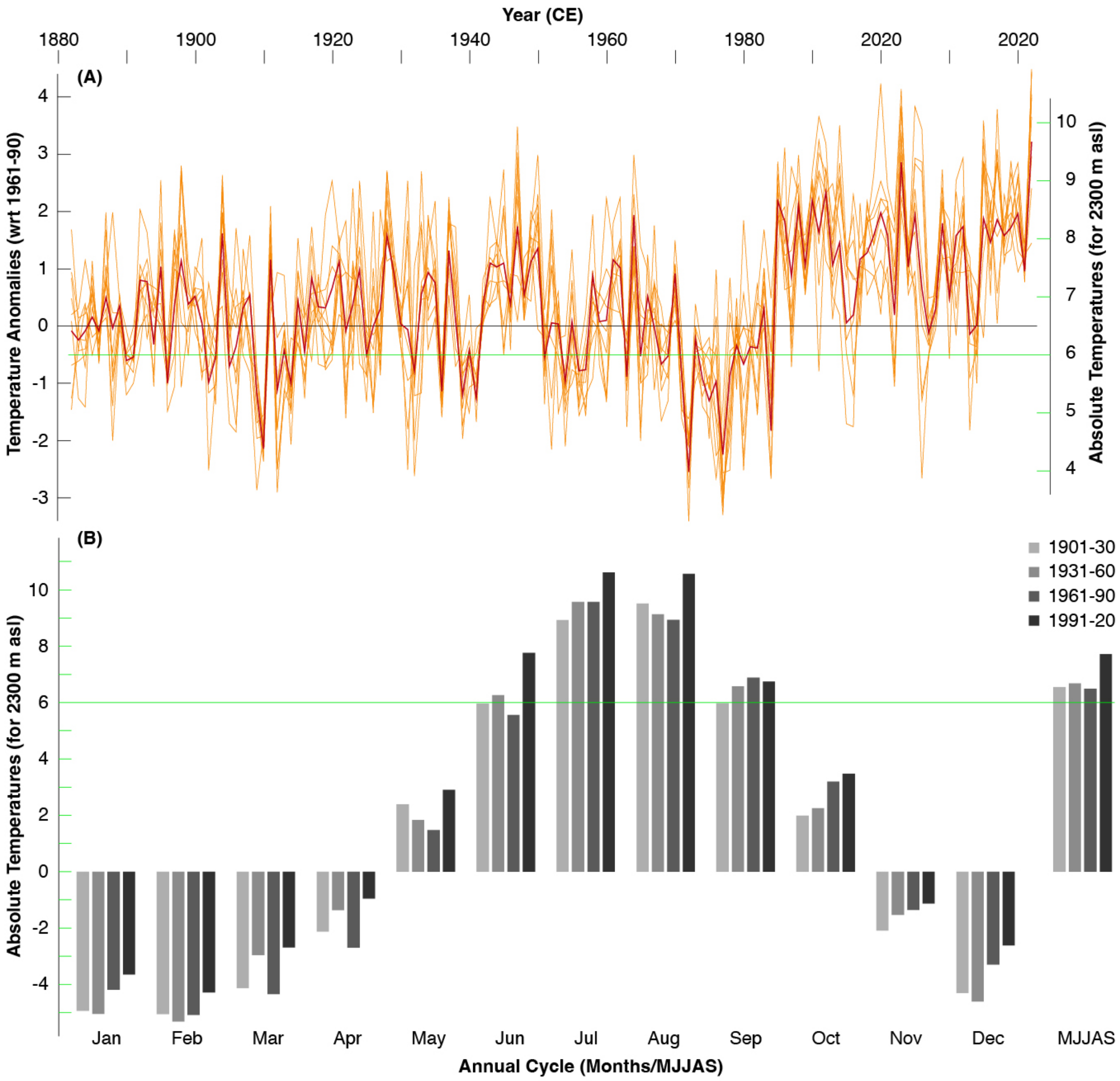

Figure S7. Station measurements. (**A**) Ten seasonal temperature means of at least two consecutive monthly mean values between May and September measured at the high-elevation Pic du Midi observatory (see Fig. 1 for details). All seasonal means are shown in orange, with the most relevant May–September (MJJAS) mean shown in dark red. All timeseries are expressed as anomalies with respect to 1961–1990 CE, and the y-axis on the right refers to re-calculated absolute temperatures for 2300 m asl, with the horizontal green line referring 'biological zero at around to 6 ° C. (**B**) Annual cycle of the re-calculated absolute monthly temperature means at 2300 m asl, with the grey scales referring to four consecutive, non-overlapping, 30-year periods between 1901 and 2020 CE.

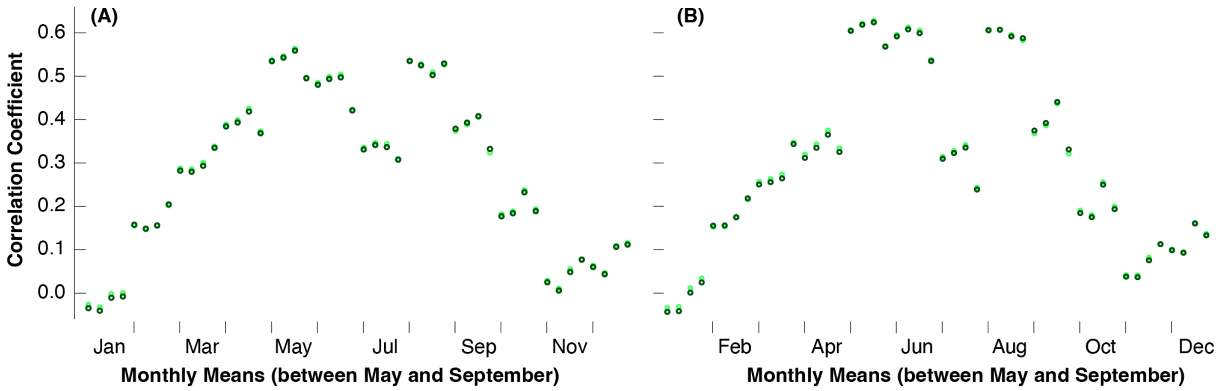

Figure S8. Monthly temperature response. (**A**) Correlation coefficients between the mean and median VSE MXD chronologies (light and dark green) calculated against monthly temperature means from the four gridded products Berkeley, CRUTEM, CRU and E-OBS (left to right) over the common period 1920–2020 CE. (**B**) Similar to (**A**) but restricted to 1950–2020 CE for which more agreement is found in the gridded products.

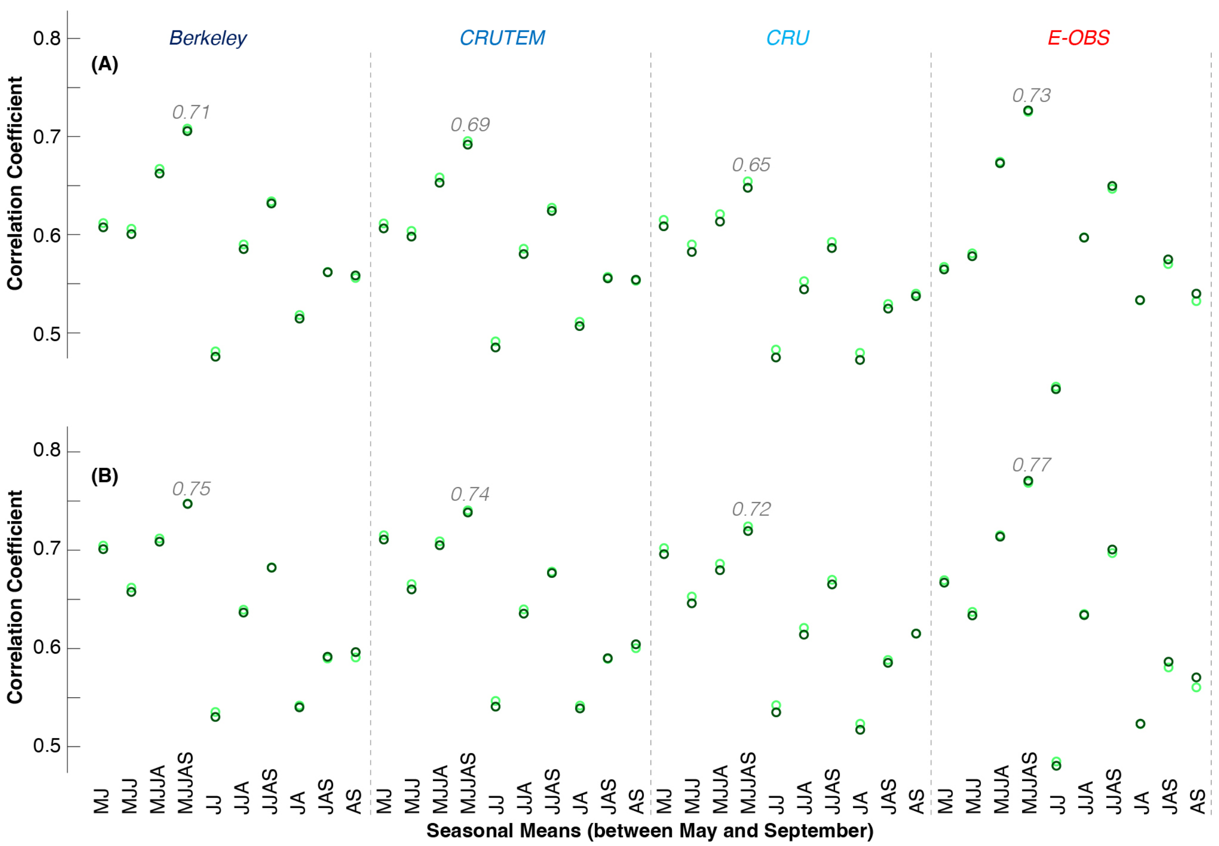

Figure S9. Warm season temperature response. (**A**) Correlation coefficients between the mean and median VSE MXD chronologies (light and dark green) calculated against seasonal temperature means between May and September over the common period 1920–2020 CE and using four gridded products (Berkeley, CRUTEM, CRU and E-OBS). (**B**) Similar to (**A**) but restricted to 1950–2020 CE for which more agreement is found in the gridded products. The ten seasonal temperature means of at least two consecutive monthly mean values between May and September are: May–June (MJ), May–July (MJJ), May–August (MJJA), May–September (MJJAS), June–July (JJ), June–August (JJA), June–September (JJAS), July–August (JA), July–September (JAS), and August–September (AS).

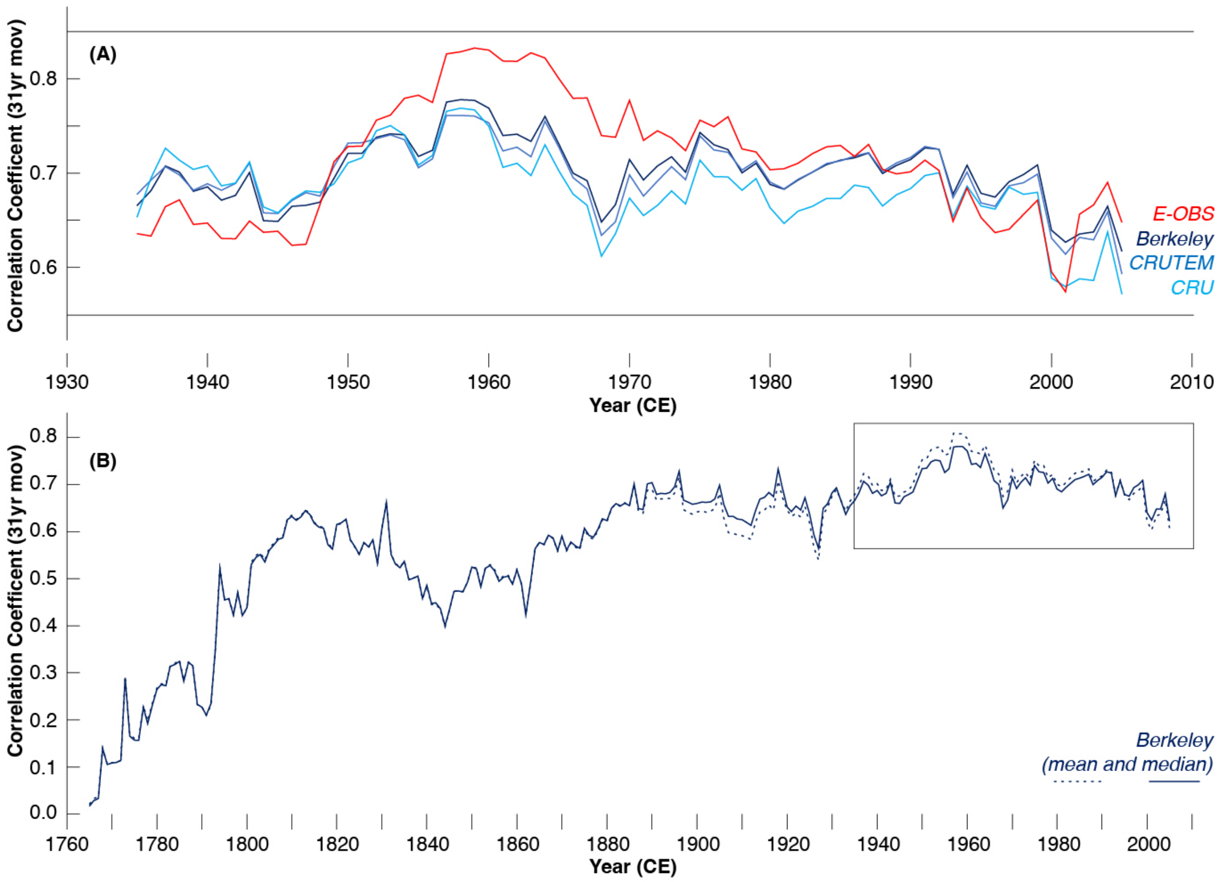

Figure S10. Temporal changes in temperature response. (**A**) Moving 31-year correlation coefficients between the median VSE MXD chronology and May–September (MJJAS) temperature means of four gridded products (Berkeley, CRUTEM, CRU and E-OBS) calculated over the common period 1920–

2020 CE. (**B**) Moving 31-year correlation coefficients between the median VSE MXD chronology and the mean and median of the gridded MJJAS temperatures back to 1760 CE.

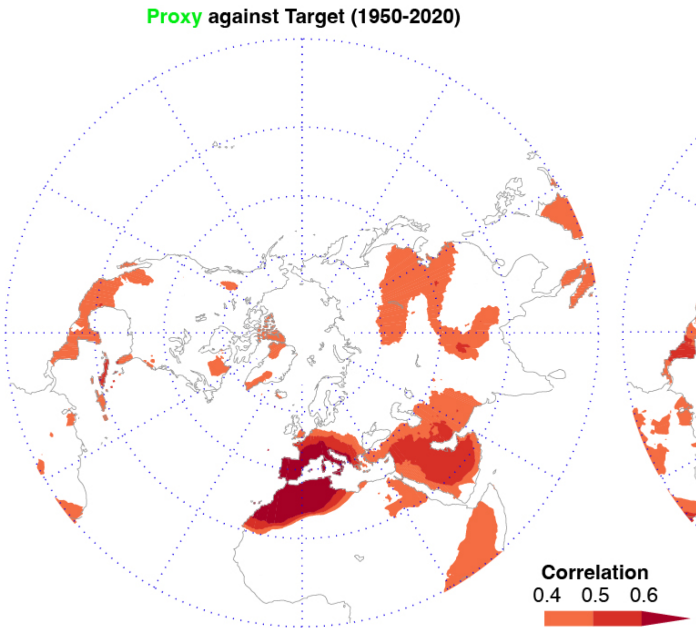

Figure S11. Hemispheric temperature signal. Spatial correlation coefficients between our new reconstruction/Pic du Midi station (left/right) and gridded (0.5° lat/lon) Norther Hemisphere land surface May–September (MJJAS) temperatures from CRU (1950–2020 CE).

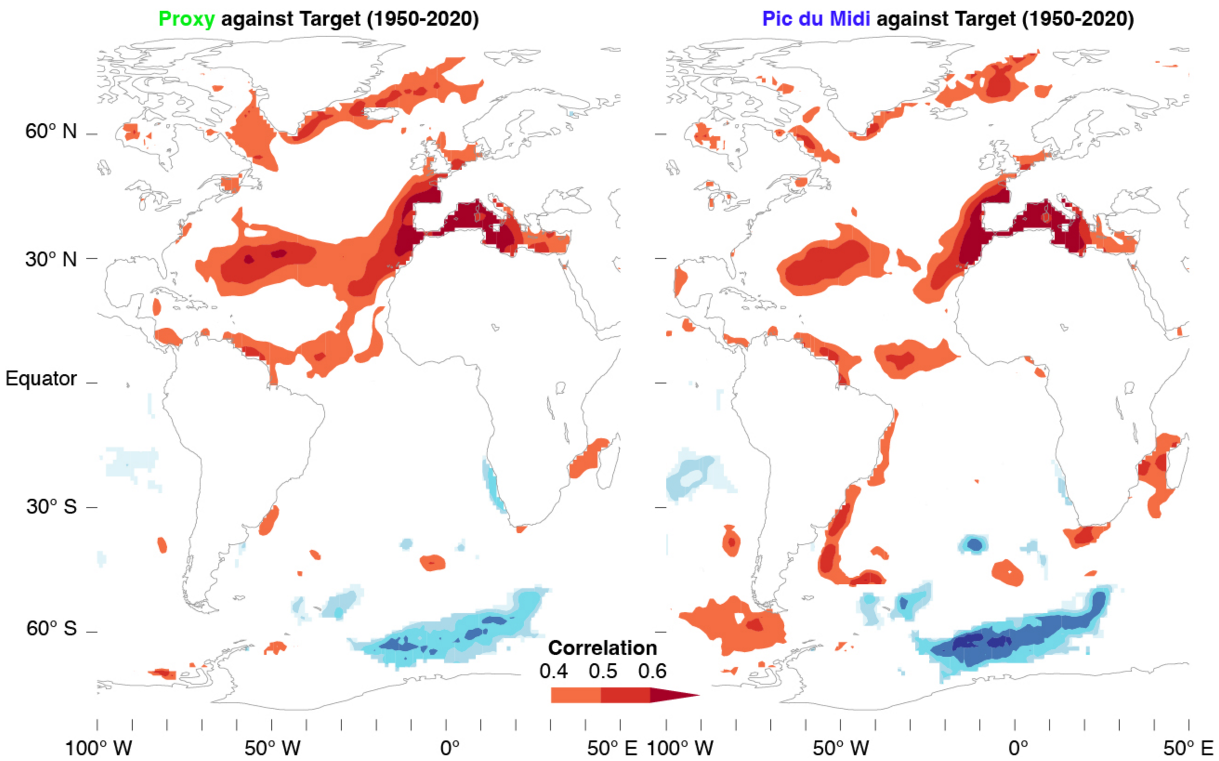

Figure S12. Oceanic temperature signal. Spatial correlation coefficients between our new reconstruction/Pic du Midi station (left/right) and gridded (1.0° lat/lon) sea surface May–September (MJJAS) temperatures from HadISST (1950–2020 CE).

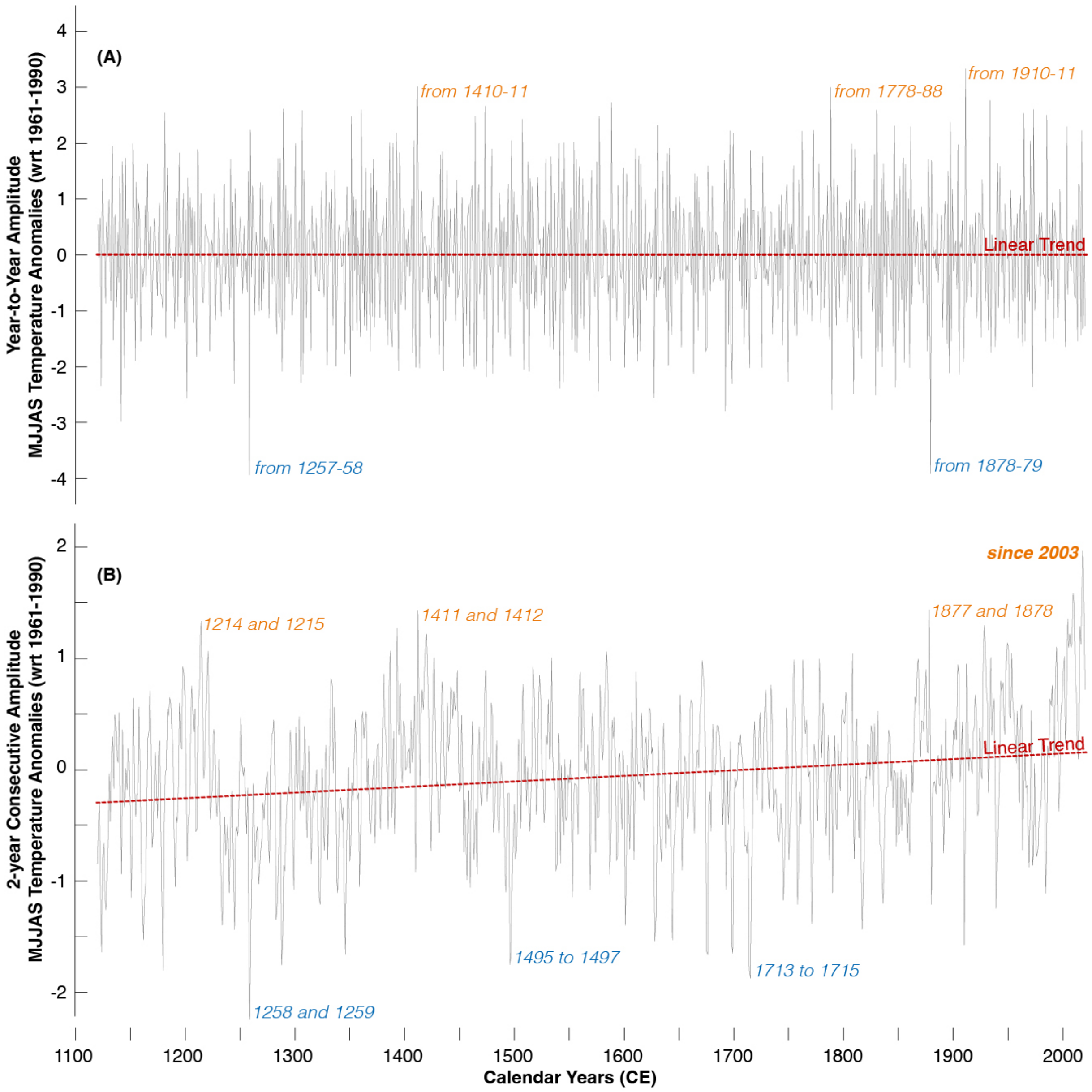
(A)
Year-to-Year Amplitude
MJJAS Temperature Anomalies (wrt 1961-1990)
from 1410-11
from 1778-88
from 1910-11
Linear Trend
from 1257-58
from 1878-79
(B)
2-year Consecutive Amplitude
MJJAS Temperature Anomalies (wrt 1961-1990)
since 2003
1214 and 1215
1411 and 1412
1877 and 1878
Linear Trend
1495 to 1497
1713 to 1715
1258 and 1259
Calendar Years (CE)

Figure S13. Year-to-year temperature changes. (**A**) Yearly amplitude of our new reconstruction (i.e., first difference), with the largest negative and positive year-to-year changes labelled. (**B**) Multi-year amplitude of our new reconstruction (i.e., at least two consecutive summers), with the largest negative and positive changes labelled.

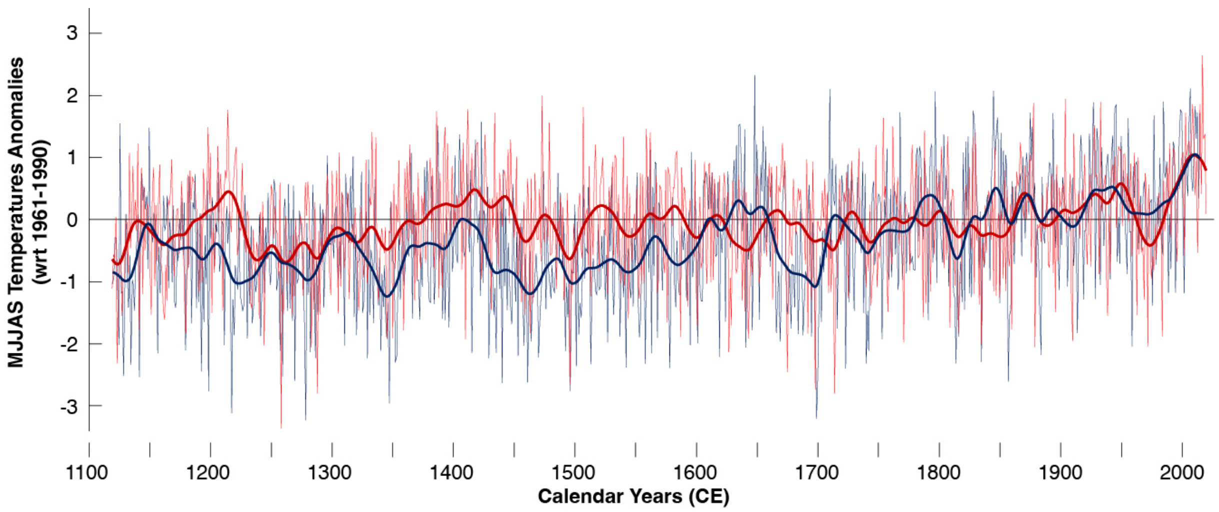

Figure S14. Mediterranean temperature reconstructions. Comparison between our new reconstruction (red) against the MXD-based July–September temperature record from Mount Smolikas in northern Greece (Esper et al. 2020). Thick lines are 50-year cubic smoothing splines.